Journal of Energy Storage 55 (2022) 105744

Contents lists available at ScienceDirect

Journal of Energy Storage

journal homepage: www.elsevier.com/locate/est

Research Papers

Incorporation of controllable supercooled phase change material heat storage with a solar assisted heat pump: Testing of crystallization triggering and heating demand-based modelling study

Cagri Kutlu [a,*], Emmanuel Tapia-Brito [a], Osaru Agbonaye [b], Yuehong Su [a], Stefan Thor Smith [b], Ben Hughes [c], Saffa Riffat [a,*]

[a] Department of Architecture and Built Environment, University of Nottingham, University Park NG7 2RD, UK
[b] School of Built Environment, University of Reading, Whiteknights House, Reading, RG6 6AH, UK
[c] Department of Engineering, University of Hull, Hull HU6 7RX, UK

ARTICLE INFO

Keywords:
Building heating demand
Latent heat storage
Supercooled PCM
Crystallization triggering of PCM
Solar-assisted heat pump

ABSTRACT

In short to long-term heat storage, the heat loss of common phase change material (PCM) systems is a big problem where heat is lost continuously to the ambient environment and is thus wasted, even when the system is not in use. Controllable supercooled PCM in the proposed system offers a solution to this problem. Latent heat is only released when the supercooled PCM is triggered to induce crystallization, so it can be stored at ambient temperature. To control the release of heat, the installation will be constructed as a group of PCM storage units, each with its own trigger, which can be activated according to the heating demand of a building perhaps over several days. The proposed versatile PCM energy storage system can play an essential role in synchronizing energy demand and supply, on a short to long-term basis (days/weeks). In this study, an electrical triggering mechanism is constructed and tested in the laboratory to control the crystallization of the PCM. The PCM temperature increased from 20 $^{\circ}C$ to 56.4 $^{\circ}C$ in 20s after triggering. After validation of controllable crystallization and melting time, a solar-assisted heat pump coupled with supercooled PCM storage units was simulated considering the heating demand profile of an eco-house in Nottingham, UK. The charging time of the PCM tank was found 6.5h when 8 cm diameter PCM tubes were adapted. During discharging period, the hot water supply temperature was achieved at higher than 43 °C, considering the one-day heating profile of the building.

1. Introduction

The increment in global total energy consumption is one of the concerns regarding the fight against the effects of global warming. The energy consumption in buildings is considered as an increasing proportion of total energy consumption around the world [1]. It has been reported that 32.5% of the UK energy usage is consumed by buildings [2], this figure increases to 40 % of final energy consumption in the European Union [3]. Within energy usage, space heating is the most important end-use in buildings at 68 % [4]. Since space heating is also a source of a high proportion of carbon emissions, using more efficient systems or renewable energy sourced units could contribute to decrement in carbon release. Heat pump technology has been an option for space heating applications because of its low electricity consumption compared to electrical heaters [5]. It is also an environmentally friendly system with zero direct carbon release against gas boiler systems. However, consumption of the heat pumps from the grid electricity also causes carbon emissions because of carbon-based fuel burning for electricity generation. Thus, solar assisted heat pumps have been introduced for higher coefficient of performance (COP) by utilizing solar energy. In this way, evaporation temperature is increased and compressor load can be reduced compared to conventional air source heat pumps [6]. However, there is a mismatch between heating demand from the buildings and available solar energy because of the nature of the solar energy, it is intermittent, and the system needs a storage unit to provide the required heating to the building. Thermal energy storage integration to the systems can help and efficiently use the energy, especially the utilization of renewable energy sources in the building energy infrastructure [7], in this way, greenhouse gas emissions can be reduced and may lead the systems to more sustainable energy systems.

Phase change materials (PCM) provide a functional approach as a

* Corresponding authors.
E-mail addresses: cagri.kutlu2@nottingham.ac.uk (C. Kutlu), saffa.riffat@nottingham.ac.uk (S. Riffat).

https://doi.org/10.1016/j.est.2022.105744
Received 11 April 2022; Received in revised form 5 September 2022; Accepted 21 September 2022
Available online 30 September 2022

Nomenclature

A_{col}	Collector area, m^2
c_1	Heat loss term, W m^{-2} K^{-1}
c_2	Heat loss term, W m^{-2} K^{-2}
c_p	Specific heat, J kg^{-1} K^{-1}
D	Diameter, m
G	Solar irradiance, W m^{-2}
h	Specific enthalpy, J kg^{-1}
h_{w-PCM}	Heat transfer coefficient, W m^{-2} K^{-1}
L	Heat of fusion, kJ/kg
$\dot{m}$	Mass flow rate, kg/s
M	Mass, kg
Nu	Nusselt number
P	Pressure, kPa
Pr	Prandtl number
Ra	Rayleigh number
$\dot{Q}$	Heat rate, W
T	Temperature, $^{\circ}C$
$\overline{T}$	Mean temperature in collector, $^{\circ}C$
U	Overall heat transfer coefficient, W m^{-2} K^{-1}
V	Volume, m^3

Greek letters

η	Efficiency
ρ	Density, kg m^{-3}
ϕ	PCM liquid fraction
λ_{eff}	Effective thermal conductivity, W m^{-1} K^{-1}

Subscripts

am	Ambient
col.	Collector
comp	Compressor
cond	Condenser
dis	Discharge
htf	Heat transfer fluid
is	Isentropic
r	Refrigerant
st	Storage
suc	Suction
n	Node number
w	Water
t	Tank

Abbreviations

COP	Coefficient of performance
DHW	Domestic hot water
HP	Heat pump
HTF	Heat transfer fluid
IAM	Incident angle modifier
IESVE	IES Virtual Environment
PCM	Phase change material
LHTES	Latent heat thermal energy storage
SAT	Sodium acetate trihydrate

latent heat thermal energy storage (LHTES) which can reduce the storage size compared to sensible storage options by maintaining high energy density. However, the PCM tends to have low thermal conductivity, as a result of this, the rate of energy extraction and delivery is limited. Therefore, PCM storage design must provide the instantaneous heat transfer rate required by the system [8]. Among different ways of containing the PCM such as immersed heat exchangers and macro encapsulation, macro-encapsulation technique presents good stability and cost-effectiveness [9]. Different geometries have been investigated regarding improvement of heat transfer rate in macro encapsulated PCM. Xu et al. [10] showed that using ellipsoidal capsules discharge time can be lessen 60 % but storage capacity also decreases by 23 % compared to off-the-shelf cylindrical PCM capsules. In literature, the integration of LHTES devices with heat pump units has been investigated. The aim of this combination is to shift the peak load which can also result in reducing the buffer tank size and synchronizing the produced heat and demand profile which can alleviate grid stress. [11]. Parallel to this, there is an increasing interest in integration of LHTES in building heating systems as a demand-side management tool [12]. In applications of space heating load management, LHTES has been implemented as a unit in the hydronic space heating systems. In these systems, the heat is provided by boilers or heat pumps and the heat is carried by water in order to heat the building space as radiator systems [13]. Since this study investigates the controlled solidification of the PCM, macro-encapsulated systems have been investigated. Applications of the use of PCM in space and water heating systems, different integration methods and configurations can be found in the literature such as cylinder tubes, spherical containers [14], rectangular PCM slabs, [15]. Considering the heat transfer area improvement and controllable heat-releasing requirements, cylindrical tubes of macro-encapsulated PCMs containers can be applicable. This selection is also common in literature studies [16].

Xu et al. [17] experimentally investigated cylindrically macro-encapsulated latent heat storage for space heating applications. They presented the effects of charging-discharging temperatures and flow rates of the heat transfer fluid. They showed that the vertical orientation of the PCM cylinders decreases the thermal capacity of PCMs by about 8.2 % due to separation. The same group also numerically investigated the thermal performance of PCM cylinders in the tank for residential heating [18], the results showed that decreasing capsule diameter from 69 mm to 15mm shorten charging/discharging times from 12.5 h/9.8 h to 5.2 h/3 h. Another study simulated the dynamic load shifting performance of the PCM tank [11]. They presented that using the daytime charging strategy, the indirect CO_2 emissions can be reduced by up to 14%. Li et al. [19] integrated PCM tubes into a square water tank and investigated the temperature variation characteristics and the heat discharge performance of the PCM tank and conventional tank. They reported that instantaneous heat supply can be improved by 45.6 % compared to the conventional water tanks on average and they suggested using lower flow rates for discharging. As a similar PCM tank concept, Kozelj et al. [20] improved thermal storage tank capacity by encapsulated PCMs in cylindrical nodules. Their experimental analysis showed that 15% of the PCM placed into the tank increases heat storage by 70% over conventional water tanks. Jin et al. [21] experimentally evaluated solar-heat pump latent heat storage performance by using cylindrical PCM tubes in the tank, the overall performance was increased by 57.5 % compared to the air source heat pump. As latent heat storage units show promising outcomes with their outstanding large heat capacity, however, Shirinbakhsh et al. [22] presented that embedding PCMs in the storage tanks is not a promising solution as the system performance is dependent upon the operating conditions. Thus, realistic operation conditions and demand profiles are the key indicators of system performance.

Moreover, for long-term storage, heat losses of the conventional PCM systems are still a considerable problem where heat is lost continuously to the ambient environment and is thus wasted, even when the system is not in use. Supercooled PCMs offer a solution to this; latent heat is only released when triggered to induce crystallization, even when stored at ambient temperature. In applications of heat storage systems, the supercooling state is generally considered a drawback, because it

prevents the release of latent heat [23]. Thus, many studies have investigated ways of preventing or controlling the degree of supercooling such as using additives to limit supercooling [24]. In this way, regulation of supercooling and optimization of thermal properties can be achieved [25]. However, supercooling with controllable crystallization by externally triggering can be a promising phenomenon as latent heat is only released when triggered. This special feature thus provides PCM installation that can be beneficially integrated with intermittent renewable energy sources such as solar thermal collectors and a heat pump unit.

Regarding controllable crystallization of sodium acetate trihydrate (SAT), Englmair et al. [26] carried out a numerical study to show that solar combi-system including on-demand crystallization of supercooled SAT composites can provide 56 % annual solar fraction of heat supply according to a passive house. They showed that optimisation of sizes of the components can increase the solar fraction up to 71 %. Kutlu et al. [27] presented a simulation study of a solar assisted heat pump unit with PCM tank that controllable crystallization of SAT can reduce daily domestic hot water (DHW) energy consumption around 13 % in an average solar day. Englmair et al. [28] also demonstrated a solar combi-system utilizing SAT. They did laboratory tests using tubular collectors and segmented PCM heat storage prototype considering Danish passive house scenario. They tested different control strategies to enable the best automated system operation and they presented that 2 L/min flow rate is enough for high heat transfer fluid (HTF) temperatures for discharging.

Although SAT is very common in heating applications, the applicability of controlled heat release from the SAT by electrical triggering and integration to a solar-assisted heat pump unit still needs to be investigated. The study differs from the literature in that the concept offers weekly storage by addressing the heating on demand issue with flexible heat release and reduced heat loss. To control the release of heat, the installation can be constructed as a group of PCM tubes each with its own trigger, which can be activated according to the heating demand of the building perhaps over several days. The aim of the study is to prove that the designed system can successfully provide the required heating to the building by utilizing solar energy. The system can be charged during high solar radiation days and the stored heat is released according to heating demand on subsequent days. The flexibility in the amount of heat release and available time of storage makes the system especially suited to regions with high variability in weather conditions such as the UK. Therefore, this paper investigates the dynamic thermal behaviour of supercooled PCM integrated solar-assisted heat pump unit for heating a family house in the UK. Using real weather data, the charging/discharging characteristic of the PCM tank is investigated in detail based on the dynamic interaction between supply and demand.

2. Sodium acetate trihydrate and triggering for heat release

The ability to obtain stored thermal energy when required is a critical feature of flexible heat storage systems. SAT is quite advantageous in these kinds of applications because it allows for a regulated release of latent heat through its solidification. Thus, controlled crystallization is the key requirement of this concept and triggering methods to release the latent heat was investigated by researchers. Dropping crystals, local cooling, percussive vibration, and electric nucleation are the most investigated techniques. Among these techniques, adding SAT crystals into the supercooled SAT is one of the most common, easy and reliable methods [29]. Although dropping crystal into the container requires manual operation, Englmair et al. [30] developed a device using a step motor to insert SAT crystals into the container and successfully operated the triggering. Local cooling is suddenly cooling of some certain part of the supercooled SAT which leads to crystallization. When a small part of the supercooled SAT solidifies, the rest of the container solidifies similar to the dropping crystal method. Local cooling for solidifying the SAT was achieved by cooling the outside of the tank using liquid CO_2 [31]. Moreover, the use of the Peltier device for local cooling successfully triggered the solidification [32]. Regarding the percussive vibration method, there are some theories to explain working principles. One is that by vibrating, the concentration of SA in a certain part of the container change to another concentration level of the container which would trigger solidification. Zhou et al. [33] used percussion vibration, by dropping a steel ball to the surface of SAT container. The theory says external kinetic energy is given to the supercooled SAT and this energy can meet the requirement of the nucleation driving force and breaks the equilibrium state [29]. Triggering methods are not only valid for SAT but studies have also been published regarding other supercooled PCM's triggering addition to the aforementioned methods, agitation and dynamic high-pressure shock methods were investigated [34]. Recently, Yang et al. [35] proposed a new method of controlled crystallization of erythritol by injection of bubbles.

In order to integrate the LHTES systems in building applications, an automatic triggering is required considering the building heating demand profile. Thus, the electric triggering method is a proper method for controlling and utilizing different numbers of SAT containers. Electric triggering is a method for inducing nucleation in which a voltage is applied to the supercooled SAT. This method involves immersing an anode and a cathode in supercooled SAT. The anode emits ions that create an electric double layer which generates an electric field. The electric field induces the formation of a large SAT's gradient of concentration, which results in nucleation. Thus, electrodes play a critical role in electrical activation of SAT. Electric triggering is a low-cost and simple method that can be easily automated. Electric nucleation is a viable means of triggering. However, both theoretical and experimental study on electric nucleation is lacking. The method for achieving successful electric nucleation remains uncertain [29]. Therefore, sample was prepared in lab to test electrical triggering of the SAT.

The electrodes were prepared according to the technique given by [36], which offers a study of electrodes made of various materials for use in activating supercooled SAT. The combination of silver anode (+) and a graphite cathode (−) was selected to evaluate the effectiveness of electric triggering of supercooled sodium acetate solution. Prior treatment of the anodes was required, since they must have a thin layer of powder on their surface to start nucleation. To achieve that, the silver anode was polished with P80 grit sandpaper and dusted with SAT powder, then polished with P360 grit sandpaper and sprinkled with SAT powder again, and finally polished using P1200 grit sandpaper. Following that, the anode was immersed for 2 h in a 75 °C sodium acetate trihydrate solution to remove any remaining SAT powder. In tests, the temperature readings from 1 K-type thermocouple were recorded using an 8-channel data logger brand Grant model 2020. According to the manufacturer, the accuracy of the thermocouples is 0.05 %.

A voltage of 9 V was supplied throughout the testing, and after 1 s, nucleation began. Fig. 1a-f depict photos taken during laboratory studies of the electrically produced nucleation process and Fig. 1 g shows the temperature change of the PCM after activation. The electrodes were placed in a small transparent tube to lead the solidification in two directions. The pictures in Fig. 1 show the evolution of crystallization upon electrical activation over a period of 20s. Crystallization starts at the electrode tips and spreads from the centre until it completely covers the whole solution in the flask. The heat from crystallization of PCM firstly raises the temperature of solution before the entire solution reaches the temperature of crystallization, as indicated by the temperature curve in Fig. 1.

It can be seen from the figure that SAT temperature can reach maximum temperature in 20s and also the test indicated that the temperature can be obtained up to 56.4 °C instead of 58 °C. In the modelling works, melting and solidification temperatures will be taken as recorded temperature 56.4 °C.

2.1. Supercooled PCM storage modelling

The PCM storage unit is a cylinder shape container with a number of

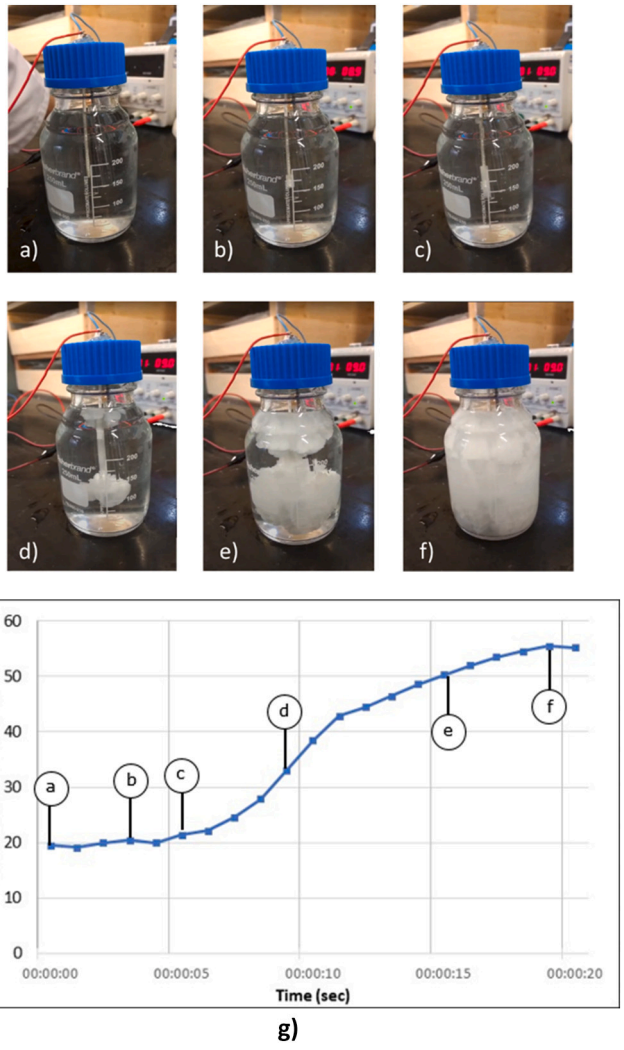

Fig. 1. (a-f) Electrical triggering of PCM at different times, and (g) temperature change of the measured point.

cylindrical PCM tubes placed inside. The horizontal direction of the PCM storage unit is divided into a number of control volumes.

To analyse the temperature gradients with heat transfer process water flow is assumed one-dimensional along the longitudinal direction. Natural convection of water is only in the radial direction. Mass transport in the tank is assumed in one dimension. Each element of the tank also contains PCM tube elements and heat transfer happens between PCM outer surface and water, thus, in a water element, water temperature and PCM temperature can be different as charging and discharging happens. The PCM tubes are also divided into radial nodes to constitute heat transfer through the PCM centre to outer edge.

Fig. 2 shows the PCM tank layout and heat transfer between nodes inside the PCM tank. For each cylindrical PCM tube, heat conduction in both radial and longitudinal directions were considered. Convection heat transfer occurs between all the PCM tubes and their surrounding water in each element. The water in each element is also exposed to convection heat loss via tank wall and conduction happens between adjacent elements.

Generalized energy equations of the PCM can be adopted from Manfrida et al. [37]:

$$V_{PCMj,n} \bullet \rho_{PCMj,n} \bullet L_{PCMj,n} \bullet \frac{\partial \phi_{j,n}}{\partial t} - V_{PCM_{j,n}} \bullet \rho_{PCM_{j,n}} \bullet c_{p,PCM_{j,n}} \bullet \frac{\partial T_{PCMj,n}}{\partial t} = \dot{Q}_{W_n-PCMj,n} + \dot{Q}_{PCM(j-1),n-PCMj,n} + \dot{Q}_{PCMj,n-PCMj,(n+1)} \quad (1)$$

j indicates radial nodes and n indicates horizontal nodes. ϕ is PCM liquid fraction, $V_{PCMj,\,n}$ is volume, $\rho_{PCMj,\,n}$ is density and $L_{PCMj,\,n}$ is the heat of fusion per unit mass of the PCM j^{th} element at horizontal node number n. $\dot{Q}_{W_n-PCMj,n}$ is convection heat transfer rate between water and the PCM element. $\dot{Q}_{PCM(j-1),n-PCMj,n}$ is conduction heat transfer rate between PCM nodes in radial direction and $\dot{Q}_{PCMj,n-PCMj,(n+1)}$ is for conduction heat transfer rate between PCM nodes in horizontal direction. Eq. (1) covers the outer PCM node in the tube but, for middle PCM nodes, convection heat transfer between water and PCM is replaced with conduction heat transfer with other radial neighbouring PCM nodes.

For the water element, energy balance equation is given in Eq. (2):

$$T_{w,n}(i+1) = T_{w,n}(i) + \frac{\dot{Q}_{cond,n}(i) + \dot{Q}_{loss,n}(i) + \dot{Q}_{W_n-PCMj,n}(i)}{M_{st,i} \bullet c_{p,w}} \bullet \Delta t \quad (2)$$

$\dot{Q}_{W_n-PCMj,n}(i)$ is convection heat transfer rate between water and PCM tube outer element in the n^{th} element, which is given by:

$$\dot{Q}_{W_n-PCMj,n}(i) = h_{wn-PCMj,n} \bullet A_{w-PCMj,n} \bullet \left(T_{w,n} - T_{PCMj,n}\right) \quad (3)$$

where $h_{wn-PCMj,\,n}$ and $A_{w-PCMj,\,n}$ are heat transfer coefficient and heat transfer area between PCM and water element, respectively. $T_{w,\,n}$ and $T_{PCMj,\,n}$ indicate water and PCM element temperatures, respectively.

Convection heat transfer coefficient covers the forced convection and natural convection during charging and discharging periods. In order to determine the convection heat transfer coefficient, natural convection heat transfer equations for spherical shapes were suggested to use for cylinders in the water tank [38]. The natural convection coefficient is found by using Nusselt number in Eq. (4):

$$Nu = \left[0.825 + \frac{0.387 \bullet Ra^{1.6}}{\left[1 + (0.492/Pr)^{9/16}\right]^{8/27}}\right]^2 \quad (4)$$

Conduction heat transfer also happens between water nodes, and it is given as $\dot{Q}_{cond,n}$:

$$\dot{Q}_{cond,n}(i) = \frac{\lambda_{eff} \bullet \pi \bullet D_t^{\,2}}{4 \bullet \Delta x} \bullet \left(T_{w,n-1}(i) + T_{w,n+1}(i) - 2 \bullet T_{w,n}(i)\right) \quad (5)$$

λ_{eff} indicates effective thermal conductivity, D_t and Δx are tank diameter and length of the water element, respectively. For λ_{eff}, 1.85 $W/(m/K)$ has been used for solar cylinders [39].

To find heat loss to the environment, Eq. (6) can be used:

$$\dot{Q}_{loss,n}(i) = U_t \bullet A_{tank,n} \bullet \left(T_{container} - T_{w,n}(i)\right) \quad (6)$$

As the PCM cylinders are in placed in a container which is in underground, the container temperature is assumed as 20 $^{\circ}C$. $A_{tank,\,n}$ indicates heat transfer area of the one node in tank. It is a surface area between water and the surrounding air of the container. U_t is overall tank heat loss coefficient.

In the modelling of SAT, the following charging, discharging, and triggering stages are shown in Fig. 3. In charging mode, PCM tubes and water in the storage tank are at 20 °C at the beginning. When the heat pump provides heating, the water and the PCM temperature increase. Sensible heating process happens and the state of PCM remains in the solid phase (point 1 to point 2). As heating continues, the state of the PCM changes from solid to two-phase and its temperature remains constant until it is completely melted (point 2 to point 3). The liquid fraction is calculated considering the latent heat capacity to determine the fully melting of each PCM element. From point 3 to point 4, the PCM element is in the liquid state, its temperature increases until point 4 and charging is completed. After charging, the PCM in the storage tank is in standby mode and it loses heat to the surrounding environment. Its temperature falls below the melting temperature but is still in liquid state thanks to supercooling. From point 5 to point 7, the PCM loses sensible heat, but latent heat capacity is also reduced as seen in Fig. 3, it

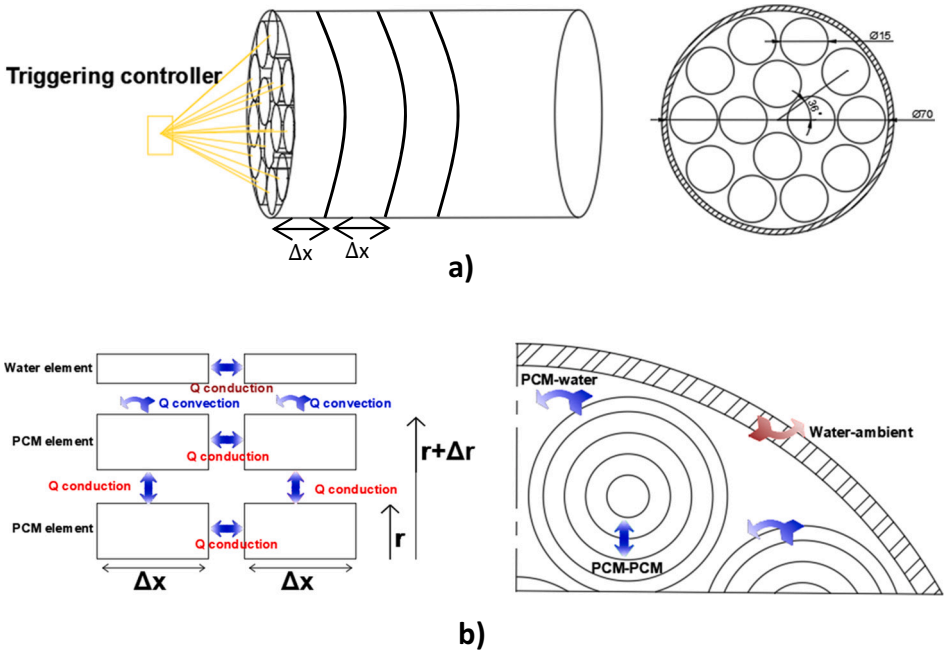

Fig. 2. (a) PCM tank layout, and (b) heat transfer diagram.

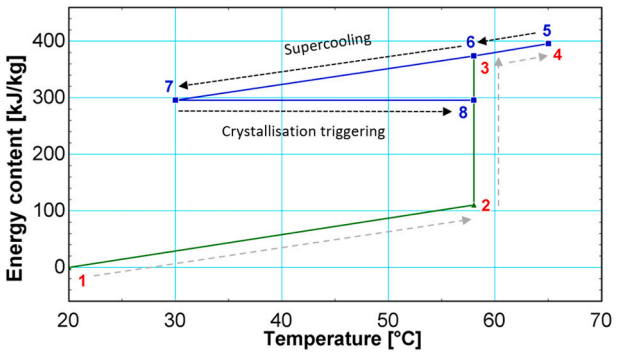

Fig. 3. Charging and crystallization triggering of SAT.

loses the energy content. In discharging mode, the PCM tubes are activated, and the need for triggering is determined by the building heating demand. Referring to the test in Fig. 1, the PCM temperature increases to melting temperature immediately (point 7 to point 8). Thus, the state of the PCM changes from liquid to two-phase considering constant enthalpy by triggering. In the model, the liquid fraction is calculated considering the lost heat during the supercooling period. The PCM element discharges its latent heat at a constant temperature until the liquid fraction falls to 0 at point 2.

The mathematical model was established by using the explicit finite-difference method. The given equations above were developed into a program in the software MATLAB. The differential items in the PCM storage tank modelling are discretized. As a result of this, the temperature changes of PCM and water in the tank at different locations are different. The PCM storage tank was divided into 40 equal elements in the longitudinal direction and the PCM tubes in each element were separated by 10 radial nodes while their surrounding water is represented by one node.

2.2. Validation of the PCM melting time

In order to validate the PCM model, transparent PCM tubes were tested to observe melting time under constant water temperature. A clear rigid acrylic pipe with 56 mm ID × 60 mm OD × 305 mm tube was filled with sodium acetate trihydrate (44wt%) and the PCM was solidified and waited to reduce solid PCM temperature until it was at room temperature. To prepare the PCM, mass of crystals was diluted with ultra-pure water, then heated to 80 $^{\circ}C$ and stirred until the crystals dissolved completely and the liquid mixture became homogeneous. Following the containers' assembly, the fluid was poured into them. To prevent crystallization of the PCM, the liquid was pushed through a funnel at a temperature of 75 °C. A sufficient air gap was left within the container to allow the PCM to expand upon solidification. In testing, the water bath temperature was set to 75 °C and when the temperature was reached to the set point, the PCM tube was placed inside the water bath. Based on visual observation, 106 min was required to fully melt the PCM. Fig. 4 shows the PCM states at beginning and after 40 min. Simulation results of the temperature changes of the given points also given below. According to simulation results, 110 min was required to fully melt the PCM however experiment shows the PCM was fully melted in 106 min. The melting tests were repeated three times and, in all tests, the errors of melting time between the model and experiment were less 5 %. When considering the simplifications of the PCM modelling, calculated time and experimental results show a good agreement.

3. System description

The overall solar assisted heat pump system consists of solar collectors, a buffer tank, a heat pump unit and PCM storage tanks. System schematic of the solar assisted heat pump with PCM storage for charging process is shown in Fig. 5a. The solar thermal collectors utilize solar energy and store it in the buffer tank. Heat pump uses collected useful heat as a heat source and boosts temperature and heat output in an efficient way. As the condensation temperature in heat pump is high enough, water is circulated between the heat pump condenser (around 70 °C) and one of the storage tanks in order to charge the PCMs. When the PCMs are charged in a storage tank, if there is still solar energy available, the circulating water is driven into the next PCM storage for charging by the control valve. In the figure, seven PCM storage tanks are shown in order to represent seven days in a week. However, it can be amended after optimisation.

When heating is requested by the building, discharging process is

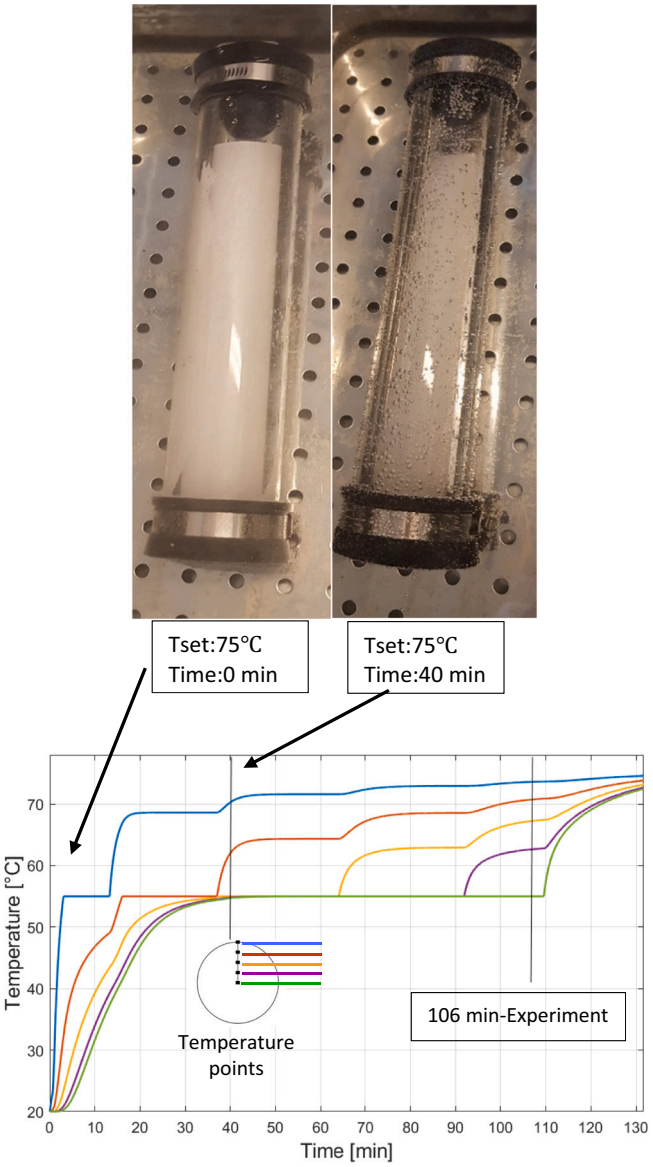

Fig. 4. PCM tube melting tests at 75 $^{\circ}C$ water bath setting.

carried out. The schematic of the discharging is shown in Fig. 5b. Since previously charged storage tank temperature is at ambient temperature, the remote-controlled triggering device activates the PCM cells and the activated PCM unit starts to crystallize immediately so, its temperature increases to phase changing temperature. Cold circulating water comes from the building enters the PCM storage tank and leaves the tank at higher temperature. Relatively higher temperature water goes into the building to be used for space heating requirement. When heating demand is too high; another PCM cell can be used by being automatically triggered.

3.1. System methodology

Proposed system is designed to provide required heating to the building by using advantage of the heat storage and solar assisted heat pump. The mathematical model is built considering the demand profile of the building. IES Virtual Environment (IESVE) [40] is used to calculate the heating demand of the selected building as the software is termed as a suite of building performance analysis tools. IESVE effectively identifies the building performance to improve by passive solutions, testing of different material integrations to reach a definite conclusion and make a decision by considering thermal comfort, energy cost and CO_2 emission control [41]. The software calculates the shading provided by surrounding objects and self-shadowing of the building, also calculates the loads from solar irradiance depending on month, time of day, geographic location of the object, its orientation. Moreover, the module allows to set thermal properties for calculating the energy loads considering created heating, ventilation, and occupancy profiles. The weather files in the software are the hourly meteorological data for a typical year for a given location. As the weather files are quite close to real conditions, the calculated heating requirement is accepted as high accuracy [42].

Fig. 6 shows the investigation methodology of the system. In the building simulation, boiler load is calculated, and the same load will be provided by the heat in the PCM storage tanks. Therefore, the heating requirement data is inserted into the MATLAB model as a demand profile. The PCM storage tank, heat pump, buffer tank and solar collector models are built in the Matlab. To use thermophysical properties of the refrigerant in the heat pump, REFPROP software is used. Moreover, weather conditions used in the IESVE are used to calculate solar collector performance and stored useful heat in the model.

4. System modelling

The modelling work includes modelling of the components such as building, solar collector, buffer tank, heat pump and PCM storage tank. The building energy modelling results are tabulated and integrated into the main model. The time-dependent transient models are built in MATLAB environment.

4.1. Heating requirement of the building

The building model is carried out by IESVE software. A case study is conducted to calculate heating loads and Fig. 7 shows the selected building for the simulation. The house is one of the Creative Energy Homes at University of Nottingham on Park Campus as well as other several low-carbon buildings. The David Wilson Eco-house is a two-story office building with dimensions of 7.9 m × 7.9 m × 5.0 m with interior floor area of 62.41 m^2 for each floor. The IESVE model uses real Nottingham, UK yearly data and real fabric materials used in the building. However, the house is assumed as a family dwelling for 2 professional parents and 2 children in school ages. The occupancy profile, heating profile, ventilation rates, appliances profile and lighting profile are designed accordingly for the mentioned 4people.

The materials and their thermal performance specifications were implemented into the model. The main construction elements and U-values are given as: External wall 0.22 W/m^2K, roof 0.19W/m^2K, glazing 1.8 W/m^2K, door 2.2 W/m^2K and floor 0.2 W/m^2K.

The heating and occupancy profiles are designed according to the real life and simplified to be the same throughout the 1 year. Weekdays and weekend profiles are set separately. In weekdays, everyone leaves the house at 07:30and comes back home at 18:00. It is also assumed that all family members stay at home during the weekends. Heat gain from occupants is 90 W/person sensible and 60 W/person latent. Lighting and appliances profiles are the same with the occupancy profiles except sleeping periods. General lightings and all appliances' heating gain is total 530W. Natural ventilation is 5 L/s/person, and infiltration rate is taken as 0.3 ach. Heating profile is designed as follows: Set temperature of the rooms is 18 $^{\circ}$C from 22:00 to 05:30since winter operating conditions of bedrooms are recommended 17–19 $^{\circ}C$ by CIBSE guide [43]. When all house members are outside, the set temperature is reduced to 15 $^{\circ}C$, by this way, heating may not require during unoccupied hours (7:30 to 18:00). In the remaining times, the set temperature is assigned as 21 $^{\circ}$C to make an average temperature of kitchen, hall, bed rooms and living rooms [43].

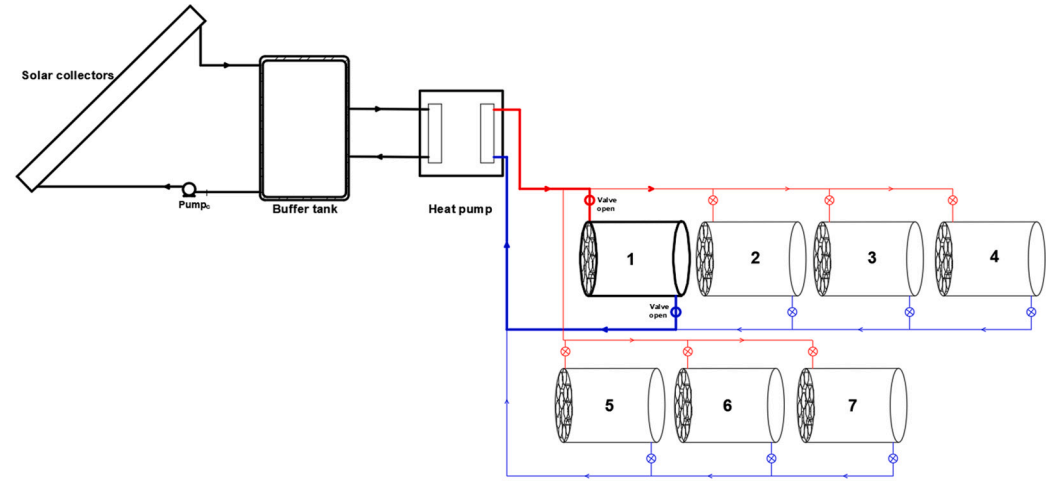

a) Charging

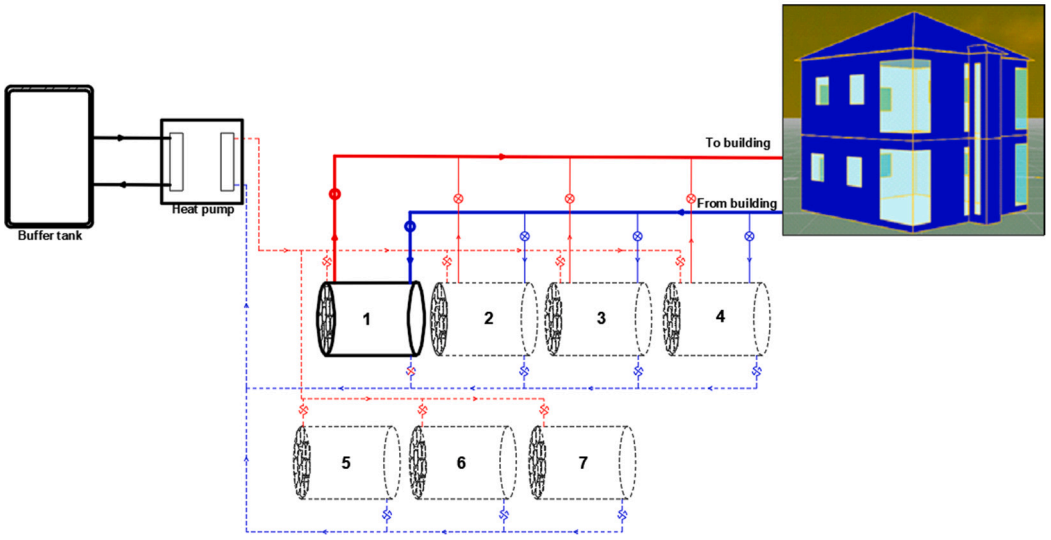

b) Discharging

Fig. 5. System schematic of the solar assisted heat pump unit with PCM storage for (a) charging, and (b) discharging.

4.2. Solar collectors

The solar collector system modelling considers quasi-steady state conditions by neglecting thermal capacity of the collectors [44]. Eq. (7) is thermal efficiency equation of the collector.

$$\eta_{col} = \eta_0 - c_1\frac{\overline{T} - T_{am}}{G} - c_2\frac{(\overline{T} - T_{am})^2}{G} \tag{7}$$

where η_0, c_1, $\overline{T}$, T_{am} and G are zero-loss efficiency, collector heat loss coefficient, mean water temperature in the collector, ambient temperature, and solar radiation, respectively. The incident angle modifier (IAM) factors applied to the zero-loss efficiency, the parameters for Thermomax HP-200 evacuated-tube heat pipe collector [45]. The modification of the thermal efficiencies under London conditions were taken from Freeman et al. [44]. The zero-loss efficiency and heat loss coefficients are $\eta_0 = 0.556$, $c_1 = 0.888$, $c_2 = 0.006$. In order to calculate useful heat and collector outlet temperature, Eq. (8) can be used:

$$\dot{Q}_{col} = \eta_{col} \bullet A_{col} \bullet G = \dot{m}_{htf} \bullet c_{p,htf} \bullet \left(T_{col,out} - T_{col,in}\right) \tag{8}$$

where A_{col} is collector area. $\dot{m}_{htf}$ and $c_{p,\,htf}$ refer circulating water mass flow rate and specific heat, respectively.

4.3. Buffer tank

Collected heat by the solar collectors is stored in a buffer tank. In order to avoid freezing, Ethylene Glycol water mixture is filled in the buffer tank as in real applications. The buffer tank is exposed to charging by collectors and discharging by heat pump when they are in operation, besides exposed to ambient heat losses during the days. Transient performance of the buffer tank is modelled by considering stratification. One-dimensional temperature distribution model is applied [46,47]. The buffer tank volume is divided into equal liquid elements to obtain the temperature distribution in the storage tank. Each element is solved simultaneously, and the temperature distribution is determined. Eqs. (9)–(11) are given for the energy balance equations of the liquid elements:

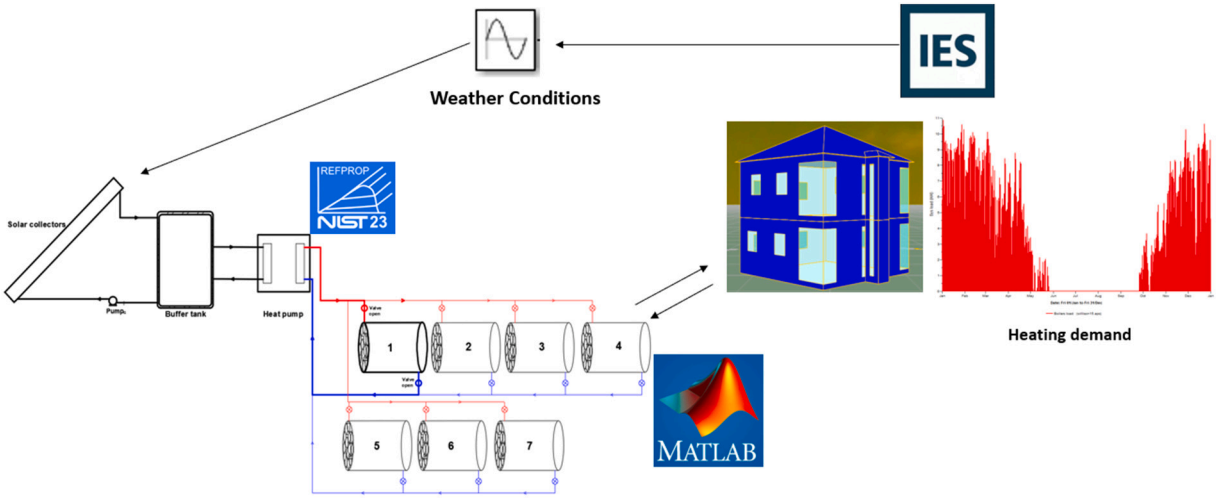

Fig. 6. Performance investigation methodology of the system.

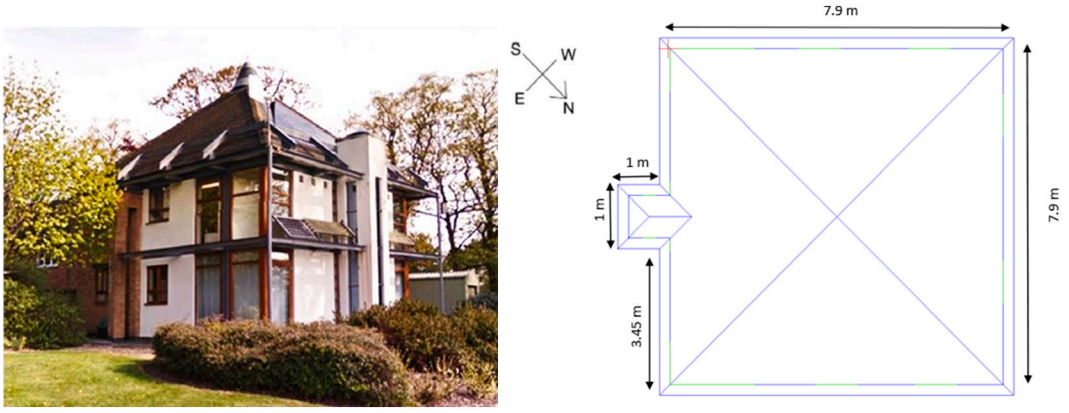

Fig. 7. The David Wilson Eco-house (left) and floor layout (right).

$$M_{st1} \bullet c_{p,htf} \bullet \frac{\partial T_{st1}}{\partial t} = \dot{m}_{c,htf} \bullet c_{p,c,htf} \bullet \left(T_{col} - T_{st,1}\right) + \dot{m}_{hp,htf} \bullet c_{p,hp,htf} \bullet \left(T_{st,2} - T_{st,1}\right) - U_t \bullet A_{st1} \bullet \left(T_{st,1} - T_{am}\right) \quad (9)$$

$$M_{st,i} \bullet c_{p,htf} \bullet \frac{\partial T_{st,i}}{\partial t} = \dot{m}_{c,htf} \bullet c_{p,c,htf} \bullet \left(T_{st,i-1} - T_{st,i}\right) + \dot{m}_{hp,htf} \bullet c_{p,hp,htf} \bullet \left(T_{st,i+1} - T_{st,i}\right) - U_t \bullet A_{st,i} \bullet \left(T_{st,i} - T_{am}\right) \quad (10)$$

$$M_{st,N} \bullet c_{p,htf} \bullet \frac{\partial T_{st,N}}{\partial t} = \dot{m}_{c,htf} \bullet c_{c,htf} \bullet \left(T_{st,N-1} - T_{st,N}\right) + \dot{m}_{hp,htf} \bullet c_{p,hp,htf} \bullet \left(T_{hp,htf} - T_{st,N}\right) - U_t \bullet A_{st,N} \bullet \left(T_{st,N} - T_{am}\right) \quad (11)$$

where $\dot{m}_{c,htf}$ and $\dot{m}_{hp,htf}$ are heat transfer fluid mass flowrate coming from the solar collectors and heat pump, respectively, $T_{hp,\,htf}$ is returning heat transfer fluid temperature from the heat pump and it is charged to the tank bottom element, U_t indicates the thermal loss coefficient of the thermally-insulated cylinder.

4.4. Solar assisted heat pump

Solar assisted heat pump unit both provide heating for PCM storage charging and direct heating to the building in order to compare the effect of PCM storage integration into the system. The heat pump consists of four main components namely, compressor, condenser, expansion valve and evaporator. The schematic of the solar assisted heat pump unit with building system is given in Fig. 8.

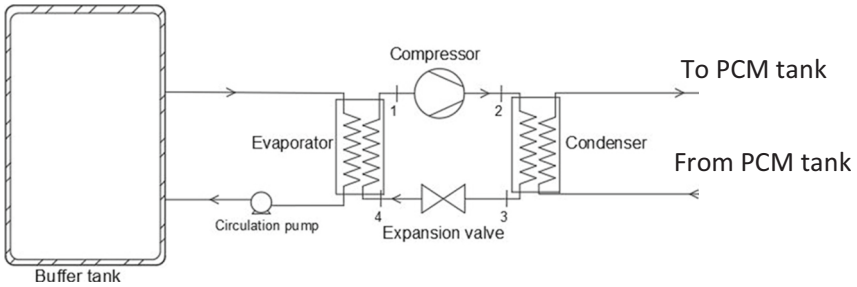

Fig. 8. Solar assisted heat pump components.

The solar assisted heat pump units in the market mostly come with a buffer tank to utilize solar energy in maximum level. Thus, heat transfer fluid coming from the buffer tank is circulated through the evaporator of the heat pump. The collected heat is used as energy source for the heat pump. In the modelling, maximum condensation temperature is fixed at 75 °C to maintain the PCM tank temperature around 70 °C. However, evaporation temperature changes by buffer tank temperature and compressor power consumption changes with the operating conditions. Eq. (12) gives compressor power consumption of the heat pump.

$$\dot{W}_{comp} = \dot{m}_r \bullet (h_2 - h_1) \Big/ \eta_{mec} \tag{12}$$

where, η_{mec} is mechanical efficiency of the compressor, it is taken 0.95 [48] and isentropic efficiency of the compressor is calculated from Eq. (13) [49]:

$$\eta_{is} = 0.874 - 0.0135 \bullet \frac{P_{dis}}{P_{suc}} \tag{13}$$

The COP of the heat pump is defined as follows:

$$\mathrm{COP} = \frac{\dot{Q}_{cond}}{\dot{W}_{comp}} \tag{14}$$

For the heat pump modelling, given assumptions were considered:

- Constant pressure is assumed during condensation in the condenser and evaporation in the evaporator.
- The expansion of the refrigerant in the expansion valve is assumed as isenthalpic.
- 3 K subcooling and superheating is assumed. [50].
- For evaporator, 5 K pinch temperature difference approach is assumed [50] to ensure effective heat transfer.

Based on given assumptions and the eqs. T-s and P-h diagrams of the heat pump which uses low GWP refrigerant R1234yf is given in Fig. 9. The figures are drawn for 30 °C buffer tank temperature which yields to 23.18 °C evaporation temperature when flow rate of the HTF water is 0.33 kg/s.

5. Results and discussions

5.1. Determination of design conditions

Heating requirement of the building is determined based on IESVE simulation. Monthly heating demand and instant heating demand of the building for a year period have been calculated. The maximum heating requirement is found as 1.49 MWh in January; however, design month is chosen as February in order to avoid oversizing of the system because designing for February would cover all heating months except January (covers its 72 %). In the findings, instant heating demand reaches to 11 kW maximum, but this value is required for a very short period when heating started, later it falls to a certain value.

In order to size the system, daily heating demand needs to be determined. Fig. 10a shows weather data for the designed week which will be used for system performance analysis. Calculated heating demand profile for the week is given in Fig. 10b and c shows the design day's heating profile. Since building temperature profile is set to maintain the desired temperatures during occupation periods, heating is required in the morning and evening periods.

These two heating periods in a day provide an advantage of the controlled triggering of the PCMs to reduce heat losses from the tank to the environment. However, this issue will be investigated later. Recently, daily heating requirement of the building is found 28.8 kWh and the PCM mass is determined to provide this heating as 392.72 kg. By considering calculated PCM mass and given schematic in Fig. 2, 14 PCM tubes will be placed in the PCM storage tank with a diameter of 0.15 m and 1.1 m length. Therefore, the tank consists of 392.72 kg of PCM and 150 kg of water. Evacuated tube collectors with 50 m^2 area has been chosen for solar assisted heat pump unit. 800 L of buffer tank was adapted as a heat storage unit to provide heating source to the solar assisted heat pump unit. Collector flow rate is chosen constant rate as recommended by the manufacturer [45]. Ethylene Glycol water mixture (30 %) is circulated between the collectors and the buffer tank in order to avoid freezing. Initial design conditions and parameters and PCM specifications are given in Table 1.

5.2. Sizing of PCM tubes according to charging time

Size of the PCM tubes in the storage tank has a significant effect on charging time. In order to investigate the PCM tube size on charging performance, total PCM and water masses are kept constant. When the diameter of the PCM tubes decrease, the length of the PCM tubes and cylinder need to be increased to keep same PCM volume. At the same time, the diameter of the other cylinder should be reduced to maintain 150 l of water content. Fig. 11a shows effect of different PCM tube diameters on outer cylinder diameter and length.

Fig. 11b shows effect of different PCM tube diameters. As shown in Fig. 11b, smaller PCM tube diameters increase the length of the cylinder and heat transfer area between PCM outer surface and water. This increment improves the heat transfer rate and shortens to PCM charging time. In this analysis, water enters to the PCM tank at 70 °C, PCM tubes and water in the tank are initially 20 °C. The charging time which means 100 % of the PCMs in the tube is melted and the required time can be reduced from 13.7 h to 6.5 h by changing PCM diameter from 0.13 m to

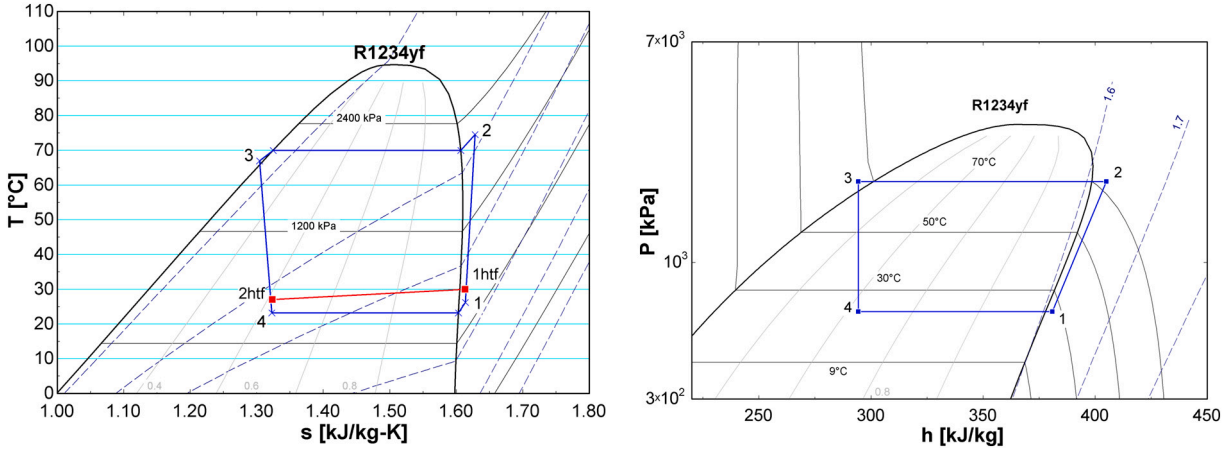

Fig. 9. T-s and P-h diagrams of the heat pump.

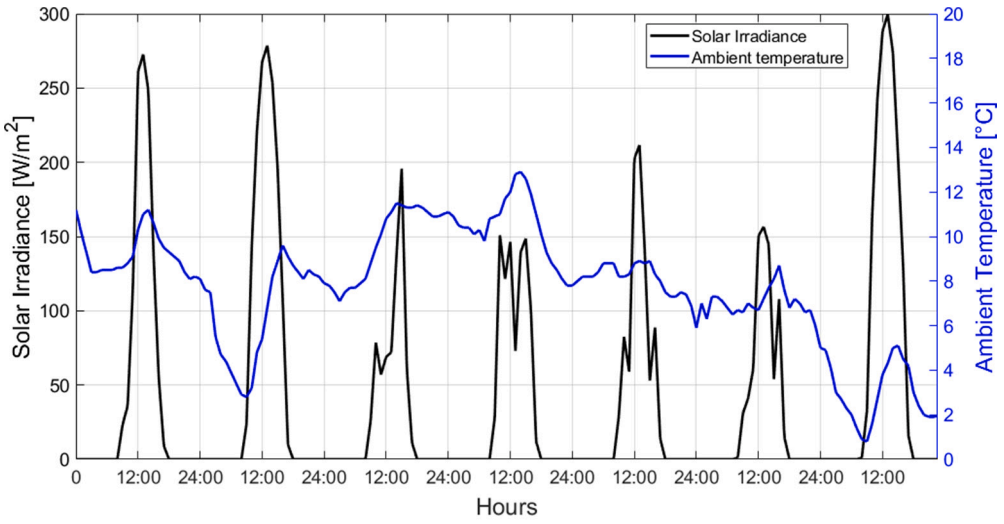

a) Solar radiation and ambient temperature during one week

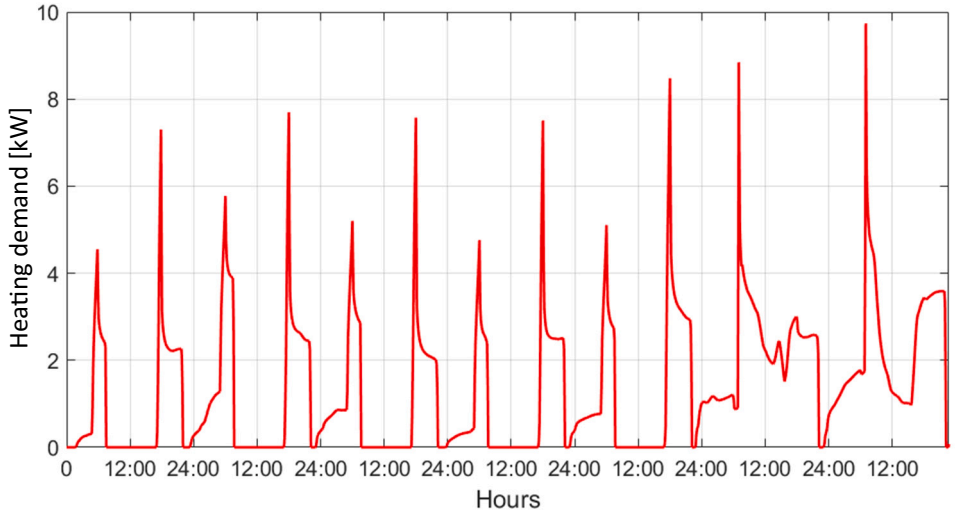

b) Heating demand profile during one week

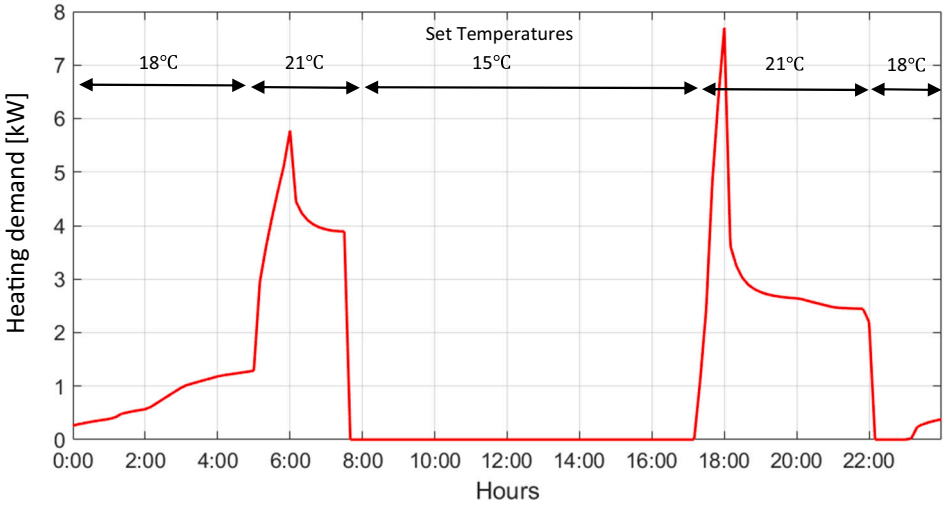

c) Design day (2nd February) heating demand profile

Fig. 10. Design weather data and heating demand profiles.

Table 1
Initial design conditions of the solar assisted heat pump with PCM storage tank.

Daily heating load	28.8 kWh	Solar collector area	50 m^2
Total PCM mass in the tank	392.72 kg	Collector flow rate	0.033 kg/s per collector
Total PCM volume in the tank	270 l	Heat Pump output	Maximum 6 kW
Charging load for PCM per day	35.79 kWh (20 °C to 56 °C)	HP condensation temperature	75 °C
Buffer tank	800 l	Pinch temperature in HP evaporator	5 °C
Buffer tank fluid	Ethylene Glycol water mixture (30 %)	Flow rate between buffer tank and HP	0.33 kg/s
Solar collector type	Evacuated tube collector	Water mass in tank	150 kg
One PCM tube volume	19.28 l	Tank heat loss coefficient	0.8 W/m^2 K [51]
PCM latent heat	264 kJ/kg [29]	PCM Specific heat	2.9/3.1 kJ/kg K [29]
PCM conductivity	0.6/0.385 W/m K [29]	PCM density	1450 kg/m^3 [29]

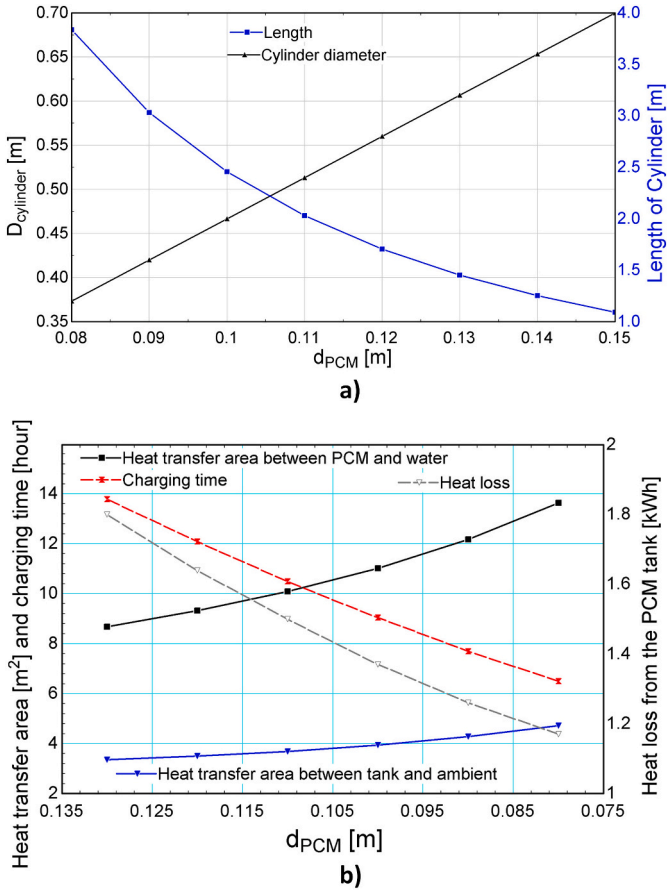

Fig. 11. (a) PCM tube and PCM tank size variations, (b) calculated heat transfer areas, charging time and heat loss to the ground.

0.08 m. However, there is a drawback of using longer cylinder as heat transfer area between tank and ambient increases as well. Since the charging time is reduced by smaller PCM tube diameter, heat loss to the ambient decreases from 1.8 kWh to 1.1 kWh for diameters of 0.13 m and 0.08 m, respectively. Thus, 0.08 m diameter is chosen.

5.3. Discharging of the stored energy

According to the scenario, previously charged PCM storage tank is activated at midnight. This operation procedure needs to be upgraded as all stored heat might not be discharged from the current tank. However, in this study, performance of heat supply of the PCM tank is simulated for different radiator water flow rates and their effect on hot water delivery temperature and PCM tank performance. Englmair et al. [26] used 7 L/min for their space heating water circulation flow. Similarly, Xu et al. [11] used 56.33 L/min flow rate for 38.8 kW heating which would be around 11.5 L/min for this study's maximum 8 kW heating demand. Surely, radiator flow rate has an impact on heating performance when heat transfer rates from the radiator to space is considered, however, the effect of circulation flow rate is investigated in this section.

By using the circulation flow rate as 10 L/min, Fig. 12a is given water temperature gradient inside the PCM tank. The water and PCM temperatures inside the tank are assumed at 30 °C at midnight when all PCM tubes are activated. After activation, the PCM temperature increases to 56.4 °C and the latent heat of the PCM heats the water. The first 2 h\ after activation, heating is not required for the house, thus, there is no water circulation. Latent heat inside the PCM tubes raises the temperature of all water elements to almost 55°C in less than an hour. When heating is required, hot water inside the tank is circulated to the radiators in the building and cooled water returns back to the PCM tank. Around 5:45, the heating requirement reaches 5 kW which causes a temperature drop in return flow, thus, the temperature of water elements close to the return water port decrease but water temperature close to the delivery port is less affected. This temperature reduction is a result of heat transfer from PCM to water that cannot compensate for the heat removal by the building despite the heat transfer is ongoing during this period with an increasing trend. Fig. 12b shows total heat transfer rate from the PCMs to the water elements. Related to water temperature variation, heat transfer rate is also changed by time and heating demand as it reaches maximum when the water temperature is lower. Around 7:30, heat demand is zero which stops the water circulation. By this way, remaining latent heat in the PCM tubes continue to increase water temperatures in the tank with a decreasing trend as the temperature difference is getting lower by time. The same temperature reduction trend of the water happens when evening heating starts. This time, the heating demand reaches more than 7 kW, and the return water temperature falls significantly that temperature of the water close to the return water port can be 36 °C.

Return water temperature affects the distribution of the water temperature in the PCM storage tank which is related to the delivery temperature to the building. Thus, the effect of different circulation water temperatures is investigated. Fig. 13 shows the delivery and return temperatures for different circulation water flow rates. Since the heat demand from the building is the same for all cases, it is clear to see that a lower flow rate yields a lower return temperature. Although this study does not investigate the heat transfer on the house side, sufficient water return temperature should be considered in order to maintain enough heat transfer rate for space heating. When the circulation water flow rate is fixed to 6 L/min, the lowest return temperature is obtained however, a higher delivery temperature is also maintained. The low flow rate causes a large temperature difference between the inlet and outlet ports of the tank as mixing and water flow in the tank is lesser. When the flow rate is increased, return flow temperature also increases but, mixing and fluid flow rate inside the PCM tank get higher. The effect of flow rate on delivery temperature is not significant in this case which is around 1 °C maximum when the flow rate changes from 6 L/min to 12 L/min. On the other hand, the return temperature is affected by up to 3 °C. Although the higher flow rate delivery temperature is slightly lower, it will be better to use a higher flow rate in order to limit the return flow temperature reduction.

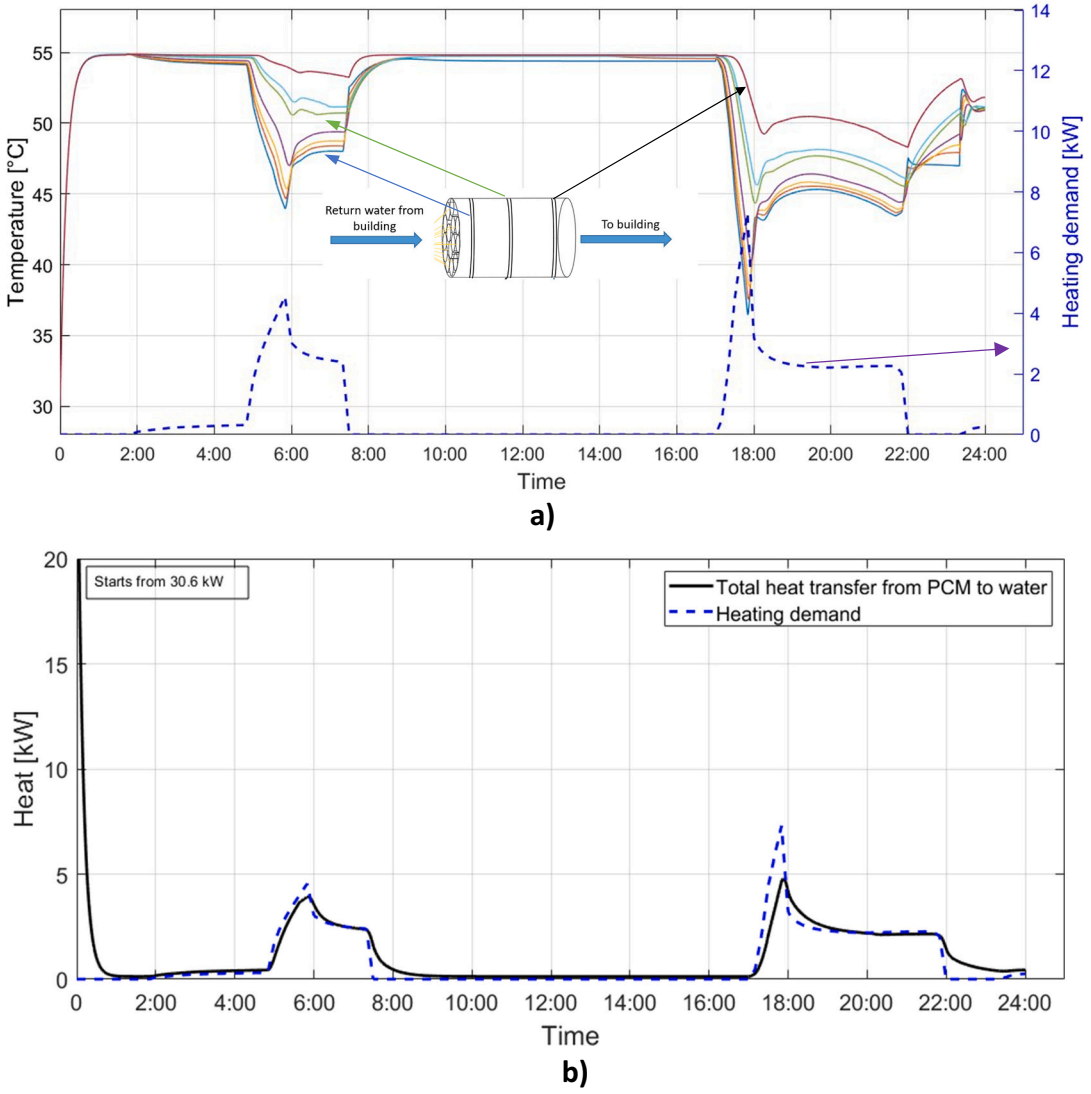

Fig. 12. Temperature variation inside the PCM tank (a) and heat transfer rate to the water (b) during the day ($\dot{m}_{radiator} = 10\,L/min$).

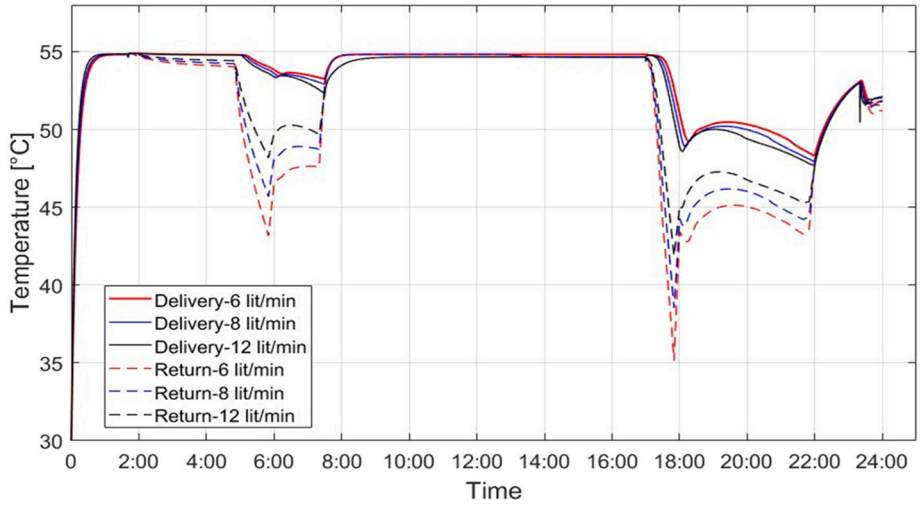

Fig. 13. Variation of water delivery temperatures to the building and water return temperatures to the PCM tank for different flow rates.

6. Conclusions

In this paper, supercooled PCM is integrated into a solar-assisted heat pump system to use a special feature of supercooling of sodium acetate trihydrate (SAT) to match the building heating demand. The advantage of using SAT is the stored latent heat can be released when triggered to induce crystallization, even when stored at ambient temperature. That makes the system promising for weather fluctuations like UK weather on weekly basis. Therefore, a number of PCM tanks can be charged by solar assisted heat pump when solar energy is available, and the charged tanks can provide heating in the following days regardless of solar radiation availability. Based on the analysis, some important conclusions from the paper are drawn as follows:

- From the controlled crystallization test, SAT temperature can reach from $20^{\circ}C$ to a maximum temperature of $56.4\ ^{\circ}C$ in 20s.
- For a required amount of PCM, the diameter of PCM tubes has an influence on PCM tank charging time as the heat transfer area changes with the tube diameter. Since the triggering action needs an apparatus in all PCM enclosures, the number of tubes was kept constant, so the length of tubes was changed correspondingly to keep the same total volume. Smaller PCM tube diameter increases the heat transfer area from the PCM to water and also heat loss from the tank. However, reduction of the charging time helps to decrease total heat loss to the ambient during the charging period. Charging time was found 6.5 h when 8 cm diameter PCM tubes were adapted.
- Effect of water circulation between the PCM tank and building has not had a significant effect on delivery temperature for the given heating profile. It changes around 1 °C maximum when the flow rate changes from 6 L/min to 12 L/min in given cases. However, it has an effect on return water temperature which should be considered to maintain sufficient heating by the radiators to the building space.
- Using 12 L/min circulation flow rate, the hot water delivery temperature was maintained higher than 43 °C considering the one-day heating load profile of the building.

CRediT authorship contribution statement

Cagri Kutlu: Investigation, Software, Writing – original draft. **Emmanuel Tapia-Brito:** Writing – review & editing. **Osaru Agbonaye:** Formal analysis. **Yuehong Su:** Conceptualization, Investigation, Writing – review & editing. **Stefan Thor Smith:** Project administration. **Ben Hughes:** Funding acquisition. **Saffa Riffat:** Project administration, Supervision, Funding acquisition.

Declaration of competing interest

The authors declare that they have no known competing financial interests or personal relationships that could have appeared to influence the work reported in this paper.

Data availability

The authors are unable or have chosen not to specify which data has been used.

Acknowledgements

The authors would like to acknowledge Engineering and Physical Sciences Research Council (EP/T02318X/1) for the financial support to this research.

References

[1] L.F. Cabeza, M. Chàfer, Technological options and strategies towards zero energy buildings contributing to climate change mitigation: a systematic review, Energy Build. 219 (2020), https://doi.org/10.1016/j.enbuild.2020.110009.
[2] Department for Business Energy and Industrial Strategy, UK energy brief in 2021 [Online]. Available, https://www.gov.uk/government/statistics/announcements/uk-energy-in-brief-2021, 2021.
[3] European Commission, Clean energy for all Europeans Package. https://ec.europa.eu/energy/topics/energy-strategy/clean-energy-all-europeans_en, 2019. (Accessed 20 October 2021).
[4] European Commission, Energy use in buildings. https://ec.europa.eu/energy/eu-buildings-factsheets-topics-tree/energy-use-buildings_en. (Accessed 21 October 2021).
[5] K.J. Chua, S.K. Chou, W.M. Yang, Advances in heat pump systems: a review, Appl. Energy (2010), https://doi.org/10.1016/j.apenergy.2010.06.014.
[6] J.G. Cervantes, E. Torres-Reyes, Experiments on a solar-assisted heat pump and an exergy analysis of the system, Appl. Therm. Eng. 22 (12) (2002) 1289–1297, https://doi.org/10.1016/S1359-4311(02)00055-8.
[7] L.F. Cabeza, et al., CO2 mitigation accounting for Thermal Energy Storage (TES) case studies, Appl. Energy 155 (2015) 365–377, https://doi.org/10.1016/j.apenergy.2015.05.121.
[8] R. Hirmiz, H.M. Teamah, M.F. Lightstone, J.S. Cotton, Performance of heat pump integrated phase change material thermal storage for electric load shifting in building demand side management, Energy Build. 190 (2019) 103–118, https://doi.org/10.1016/j.enbuild.2019.02.026.
[9] P.B. Salunkhe, P.S. Shembekar, A review on effect of phase change material encapsulation on the thermal performance of a system, Renew. Sustain. Energy Rev. 16 (8) (2012) 5603–5616, https://doi.org/10.1016/j.rser.2012.05.037.
[10] T. Xu, E.N. Humire, S. Trevisan, M. Ignatowicz, S. Sawalha, J.N. Chiu, Experimental and numerical investigation of a latent heat thermal energy storage unit with ellipsoidal macro-encapsulation, Energy 238 (2022), 121828, https://doi.org/10.1016/j.energy.2021.121828.
[11] T. Xu, E.N. Humire, J.N. Chiu, S. Sawalha, Latent heat storage integration into heat pump based heating systems for energy-efficient load shifting, Energy Convers. Manag. 236 (2021), 114042, https://doi.org/10.1016/j.enconman.2021.114042.
[12] A. Arteconi, N.J. Hewitt, F. Polonara, State of the art of thermal storage for demand-side management, Appl. Energy 93 (2012) 371–389, https://doi.org/10.1016/j.apenergy.2011.12.045.
[13] J. Heier, C. Bales, V. Martin, Combining thermal energy storage with buildings - a review, Renew. Sustain. Energy Rev. 42 (2015) 1305–1325, https://doi.org/10.1016/j.rser.2014.11.031.
[14] M.J. Li, B. Jin, Z. Ma, F. Yuan, Experimental and numerical study on the performance of a new high-temperature packed-bed thermal energy storage system with macroencapsulation of molten salt phase change material, Appl. Energy 221 (April) (2018) 1–15, https://doi.org/10.1016/j.apenergy.2018.03.156.
[15] T. Xu, et al., Performance evaluation of three latent heat storage designs for cogeneration applications, Sol. Energy 225 (June) (2021) 444–462, https://doi.org/10.1016/j.solener.2021.07.043.
[16] X. Xiao, P. Zhang, Numerical and experimental study of heat transfer characteristics of a shell-tube latent heat storage system: part I - charging process, Energy 79 (C) (2015) 337–350, https://doi.org/10.1016/j.energy.2014.11.020.
[17] T. Xu, J.N. Chiu, B. Palm, S. Sawalha, Experimental investigation on cylindrically macro-encapsulated latent heat storage for space heating applications, Energy Convers. Manag. 182 (November 2018) (2019) 166–177, https://doi.org/10.1016/j.enconman.2018.12.056.
[18] T. Xu, E.N. Humire, J.N.W. Chiu, S. Sawalha, Numerical thermal performance investigation of a latent heat storage prototype toward effective use in residential heating systems, Appl. Energy 278 (April) (2020), 115631, https://doi.org/10.1016/j.apenergy.2020.115631.
[19] J. Li, Y. Zhang, P. Ding, E. Long, Experimental and simulated optimization study on dynamic heat discharge performance of multi-units water tank with PCM, Indoor Built Environ. 30 (9) (2021) 1531–1545, https://doi.org/10.1177/1420326X20961141.
[20] R. Koželj, U. Mlakar, E. Zavrl, U. Stritih, R. Stropnik, An experimental and numerical analysis of an improved thermal storage tank with encapsulated PCM for use in retrofitted buildings for heating, Energy Build. 248 (2021), https://doi.org/10.1016/j.enbuild.2021.111196.
[21] X. Jin, H. Zhang, G. Huang, A.C. Lai, Experimental investigation on the dynamic thermal performance of the parallel solar-assisted air-source heat pump latent heat thermal energy storage system, Renew. Energy 180 (2021) 637–657, https://doi.org/10.1016/j.renene.2021.08.067.
[22] M. Shirinbakhsh, N. Mirkhani, B. Sajadi, A comprehensive study on the effect of hot water demand and PCM integration on the performance of SDHW system, Sol. Energy 159 (November 2017) (2018) 405–414, https://doi.org/10.1016/j.solener.2017.11.008.
[23] I. Shamseddine, F. Pennec, P. Biwole, F. Fardoun, Supercooling of phase change materials: a review, Renew. Sustain. Energy Rev. 158 (November 2021) (2022) 112172, https://doi.org/10.1016/j.rser.2022.112172.
[24] Y. Zhao, X. Zhang, X. Xu, S. Zhang, Research progress in nucleation and supercooling induced by phase change materials, J. Energy Storage 27 (September 2019) (2020) 101156, https://doi.org/10.1016/j.est.2019.101156.
[25] Q. Cheng, X. Cheng, X. Wang, P. Du, C. Liu, Z. Rao, Supercooling regulation and thermal property optimization of erythritol as phase change material for thermal energy storage, J. Energy Storage 52 (PC) (2022), 105000, https://doi.org/10.1016/j.est.2022.105000.

[26] G. Englmair, C. Moser, H. Schranzhofer, J. Fan, S. Furbo, A solar combi-system utilizing stable supercooling of sodium acetate trihydrate for heat storage: numerical performance investigation, Appl. Energy 242 (December 2018) (2019) 1108–1120, https://doi.org/10.1016/j.apenergy.2019.03.125.
[27] C. Kutlu, Y. Zhang, T. Elmer, Y. Su, S. Riffat, A simulation study on performance improvement of solar assisted heat pump hot water system by novel controllable crystallization of supercooled PCMs, Renew. Energy 152 (2020) 601–612, https://doi.org/10.1016/j.renene.2020.01.090.
[28] G. Englmair, W. Kong, J. Brinkø Berg, S. Furbo, J. Fan, Demonstration of a solar combi-system utilizing stable supercooling of sodium acetate trihydrate for heat storage, Appl. Therm. Eng. 166 (October 2019) (2020) 114647, https://doi.org/10.1016/j.applthermaleng.2019.114647.
[29] G. Wang, et al., Review on sodium acetate trihydrate in flexible thermal energy storages: properties, challenges and applications, J. Energy Storage 40 (May) (2021), 102780, https://doi.org/10.1016/j.est.2021.102780.
[30] G. Englmair, C. Moser, S. Furbo, M. Dannemand, J. Fan, Design and functionality of a segmented heat-storage prototype utilizing stable supercooling of sodium acetate trihydrate in a solar heating system, Appl. Energy 221 (November 2017) (2018) 534, https://doi.org/10.1016/j.apenergy.2018.03.124.
[31] M. Dannemand, J. Dragsted, J. Fan, J.B. Johansen, W. Kong, S. Furbo, Experimental investigations on prototype heat storage units utilizing stable supercooling of sodium acetate trihydrate mixtures, Appl. Energy 169 (2016) 72–80, https://doi.org/10.1016/j.apenergy.2016.02.038.
[32] G. Englmair, et al., Crystallization by local cooling of supercooled sodium acetate trihydrate composites for long-term heat storage, Energy Build. 180 (2018) 159–171, https://doi.org/10.1016/j.enbuild.2018.09.035.
[33] G. Zhou, Y. Li, M. Zhu, Experimental investigation on space heating performances of supercooled thermal storage units with sodium acetate trihydrate, Energy Build. 271 (2022), 112329, https://doi.org/10.1016/j.enbuild.2022.112329.
[34] N. Beaupere, U. Soupremanien, L. Zalewski, Nucleation triggering methods in supercooled phase change materials (PCM), a review, Thermochim. Acta 670 (October) (2018) 184–201, https://doi.org/10.1016/j.tca.2018.10.009.
[35] S. Yang, X. Shao, H. Shi, J. Luo, L. Fan, Bubble-injection-enabled significant reduction of supercooling and controllable triggering of crystallization of erythritol for medium-temperature thermal energy storage, Sol. Energy Mater. Sol. Cells 236 (November 2021) (2022) 111538, https://doi.org/10.1016/j.solmat.2021.111538.
[36] C. Dong, R. Qi, H. Yu, L. Zhang, Electrically-controlled crystallization of supercooled sodium acetate trihydrate solution, Energy Build. 260 (2022), 111948, https://doi.org/10.1016/j.enbuild.2022.111948.
[37] G. Manfrida, R. Secchi, K. Stańczyk, Modelling and simulation of phase change material latent heat storages applied to a solar-powered organic Rankine cycle, Appl. Energy 179 (2016) 378–388, https://doi.org/10.1016/j.apenergy.2016.06.135.
[38] R. Padovan, M. Manzan, Genetic optimization of a PCM enhanced storage tank for solar domestic hot water systems, Sol. Energy 103 (2014) 563–573, https://doi.org/10.1016/j.solener.2013.12.034.
[39] M. Herrando, C.N. Markides, K. Hellgardt, A UK-based assessment of hybrid PV and solar-thermal systems for domestic heating and power : system performance, Appl. Energy 122 (2014) 288–309, https://doi.org/10.1016/j.apenergy.2014.01.061.
[40] IESVE. https://www.iesve.com/software/virtual-environment, 2020. (Accessed 4 September 2021).
[41] S. Sui, R. Rasheed, Q. Li, Y. Su, S. Riffat, Technoeconomic modelling and environmental assessment of a modern PEMFC CHP system: a case study of an eco-house at University of Nottingham, Environ. Sci. Pollut. Res. 26 (29) (2019) 29883–29895, https://doi.org/10.1007/s11356-019-06054-5.
[42] V. Pukhkal, Numerical modeling of energy consumption in residential buildings, IOP Conf. Ser. Mater. Sci. Eng. 1079 (5) (2021), 052025, https://doi.org/10.1088/1757-899x/1079/5/052025.
[43] CIBSE, CIBSE guide a: environmental design, in: Environmental Design, 2016 [Online]. Available: www.cibse.org.
[44] J. Freeman, I. Guarracino, S.A. Kalogirou, C.N. Markides, A small-scale solar organic Rankine cycle combined heat and power system with integrated thermal energy storage, Appl. Therm. Eng. 127 (2017) 1543–1554, https://doi.org/10.1016/j.applthermaleng.2017.07.163.
[45] Kingspan, Direct Flow Vacuum Tube Solar Collector, 2017.
[46] J.A. Duffie, W.A. Beckman, Solar Engineering of Thermal Processes, John Wiley, 2013.
[47] C. Kutlu, J. Li, Y. Su, Y. Wang, G. Pei, S. Riffat, Investigation of an innovative PV/T-ORC system using amorphous silicon cells and evacuated flat plate solar collectors, Energy 203 (2020), 117873, https://doi.org/10.1016/j.energy.2020.117873.
[48] C. Kutlu, M. Tahir, J. Li, Y. Wang, Y. Su, A study on heat storage sizing and fl ow control for a domestic scale solar-powered organic Rankine cycle-vapour compression refrigeration system, Renew. Energy 143 (2019) 301–312, https://doi.org/10.1016/j.renene.2019.05.017.
[49] O. Brunin, M. Feidt, B. Hivet, Comparison of the working domains of some compression heat pumps and a compression-absorption heat pump, Int. J. Refrig. 20 (5) (1997) 308–318, https://doi.org/10.1016/S0140-7007(97)00025-X.
[50] G.F. Hundy, Refrigeration, Air Conditioning And Heat Pumps, 5th ed., Butterworth-Heinemann, 2016.
[51] C. Kutlu, J. Li, Y. Su, G. Pei, S. Riffat, Off-design performance modelling of a solar organic Rankine cycle integrated with pressurized hot water storage unit for community level application, Energy Convers. Manag. 166 (15) (2018) 132–145, https://doi.org/10.1016/j.enconman.2018.04.024.